FE MODELLING OF REFRACTORIES' MATERIAL PROPERTIES BASED ON 3D MICROSTRUCTURAL ANALYSIS

S. Pirkelmann, S. Sharba, G. Seifert, H. Friedrich, F. Raether
Fraunhofer HTL, Bayreuth, Germany

ABSTRACT

This paper presents a simulation-based approach to evaluate the mechanical strength of refractory materials by investigating the influence of the material's structural composition on component failure. A neural network is trained and applied for image segmentation of 3D computed tomography images of refractory samples, enabling the identification of different material components. Structural properties, such as phase fractions, porosity, grain sizes, and their spatial distributions, are extracted from the segmented images. Finite element analyses are then conducted to assess the impact of mechanical loads on the material. The relationship between the identified structural properties and the probability of failure is evaluated, providing insights into material reliability. The approach is demonstrated using commercially available B80 and SP78 refractory materials.

INTRODUCTION

The drive towards climate neutrality necessitates the quick optimization of thermal processes in terms of energy and material efficiency. Refractories play a crucial role in achieving these goals not only by enhancing functionality and prolonging service life but also by improving performance with reduced wear, and increased strength. These improvements enable the construction of lighter and more efficient structures, further contributing to energy savings and sustainability. In the systematic development of sustainable refractory materials, simulation-based methods offer significant advantages by reducing time and experimental effort. Consequently, understanding the behavior of refractory materials under stress becomes paramount, as it provides essential insights for optimizing their performance and reliability in a wide range of applications.

This paper aims to address the challenge of evaluating the mechanical strength of refractory materials by investigating the influence of material composition on component failure. By employing simulation-based techniques, it becomes possible to identify critical structural elements that contribute to component failure under various loads. The goal is to improve the reliability of new refractory materials by avoiding these critical elements.

The paper is structured as follows. The methodology begins with the acquisition of computed tomography (CT) imagery of refractory samples, allowing for non-destructive characterization of the material's microstructure. Subsequently, an image segmentation approach using a neural network is employed to accurately identify and classify the main structural components of the refractory material.

Following the segmentation, representative volume elements (RVEs) are extracted from the segmentation data and converted into meshes, enabling their utilization in finite element simulations. Finite element simulations are then conducted to analyze the stress increase within the RVEs when subjected to externally applied tensile strain, providing insights into the material's response to mechanical loading. Furthermore, macroscopic simulations of damage are performed using a 3-point bending simulation, allowing for an assessment of the material's behavior at a larger scale.

NON-DESTRUCTIVE ANALYSIS OF REFRACTORY SAMPLES

Computed Tomography imagery of B80 and SP78 refractories

We demonstrate our method using commercially available refractories: a dense refractory brick made of Bauxite B80 and a dense high alumina brick made of synthetic magnesia spinels with a high clay content Alurath SP 78. Cylindrical samples of 5 mm height and 33 mm diameter have been cut from the as-received refractory bricks. The resolution of the CT images is 24µm. Figure 1a) shows a slice through the CT image of a B80 material. The image clearly shows the very inhomogeneous microstructural compositions of the refractory material. The total volume of the samples is about 4.3cm^3 which is sufficiently large to be representative of the material at hand.

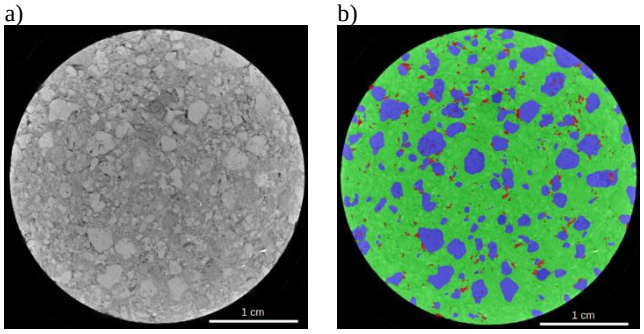

Fig. 1a): Computed tomography image of a sample of B80 refractory material with a resolution of 1518 x *1483* x *276 voxels. A single slice of the image in the z-axis is displayed. b) Segmentation image as generated by nnUNet algorithm. Different colors indicate the distinct structural components of the material: pores are shown in red, course-grained inclusions in blue, fine-grained matrix in green, background in black.*

Material analysis and 3D-image segmentation using convolutional neural networks

From the CT images, three main structural components of the refractory samples can be distinguished: pores (dark regions), coarse-grained inclusions (distinct light regions), and a fine-grained matrix in between. The structural and chemical composition of the various components of the B80 refractory was determined through scanning electron microscope (SEM) and X-ray diffraction (XRD) analysis. The analysis revealed that the B80 material consists of 61.8% Al2O3 (Corundum), 33.5% 3Al2O3-2SiO2 (Mullite), 4.6% Al2TiO5 (Tialite), with traces of other compounds. The material exhibits a complex structural composition, with distinct coarse grains made up primarily of Corundum with inclusions of either Mullite or Tialite, and varying degree of porosity. The matrix phase essentially shares the same composition but has a high degree of micro-porosity below the threshold resolution of the CT imaging.

A convolutional neural network has been trained to automate the process of generating 3D-segmentations of the CT images, assigning to each voxel of the input image a corresponding class (background, pore, distinct coarse grain, or matrix). nnUNet has been chosen for its proven effectiveness in image segmentation tasks [1]. The algorithm was trained using manually generated training data from a single B80 image, consisting of a volume of 1152×1152×64 voxels. Despite the relatively small training volume, the implementation of data augmentation strategies in nnUNet ensured the generation of high-quality segmentations. Additionally, custom variations of the input data were incorporated to replicate common CT image artifacts, enhancing the algorithm's robustness to diverse imaging conditions. The resulting segmentation, showcased in Figure 1b), demonstrates the effectiveness of the approach in accurately identifying and classifying the structural components within the B80 refractory material. The segmentation model was also applied to CT

images of the SP78 material. Despite not being specifically trained on this material, the model demonstrates excellent segmentation performance, yielding accurate results.

Analysis of structural composition

The segmentation data is used to analyze the structural composition of refractory materials. We can derive various quantities from the segmentation results such as the volume fractions of grains, pores and matrix phase, the size and local distribution of inclusions, and the orientation of particles within the matrix phase. This information can be used to compare different samples and materials based on their microstructure. To illustrate this, Figure 2 shows the volume fractions, porosity and average grain size for the B80 and SP78 samples, respectively. Note that the reported porosity only includes critical macroscopic pores that are detectable in the CT images and does not capture the much higher micro-porosity of > 10% according to density measurements.

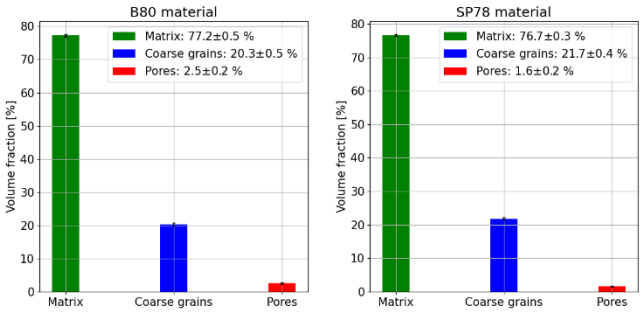

Fig. 2: Volume fractions of pores, distinct coarse grains and matrix for B80 and SP78 material.

Homogenized mechanical properties of the main structural components of the B80 material were estimated using mixture rules, as listed in Table 1. to ensure the accurate modelling of the material's behaviour under stress in the simulations.

Tab. 1: Material data used in microstructure simulations as estimated by mixture rules based on input data from the Material Property Database (MPDB) [2].

Component	Young's modulus [GPa]	Poisson ratio
Coarse grains	320	0.22
Matrix phase	95	0.22

FINITE-ELEMENT-BASED CHARACTERIZATION OF MATERIAL STRENGTH

To quantify the failure probability of a given refractory material under external load we apply finite element simulations. The analysis is focused on the B80 material, but similar investigations could be conducted for SP78.

We follow a multi-scale approach: on the micro-scale we calculate an approximate distribution of fracture stress using microstructure simulations based on representative volume elements (RVEs) extracted from the CT image segmentation data from above. The resulting distribution then serves as an input to a macro-scale simulation of a three-point bending experiment from which we can estimate the failure probability of the material.

Mesh generation from volumetric data

For the simulations on the micro-scale, we cut out numerous RVEs with a resolution of 125 x 125 x 125 voxels, each corresponding to a volume of 27 mm^3, from the segmentation image of the refractory, cf. Figure 3. For each RVE, the volumetric data is converted to a mesh for use in finite element (FE) analysis using the CGAL library [3] and subsequent simulation in Ansys APDL.

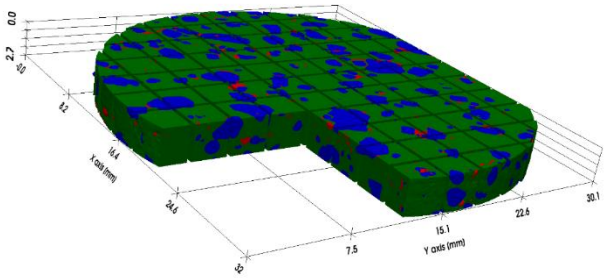

Fig. 3: Illustration of multiple representative volume elements cut from the segmented CT image of a B80 sample.

Tensile strain simulations on micro-scale

For each RVE, finite element simulations of linear elasticity were performed to determine the relative stress-increase factor compared to a defined external stress. In these simulations, a specified tensile strain was applied to the RVE, corresponding to a reference stress of 1 MPa. If structural defects such as pores are present within the RVE, the surrounding material has to bear the additional stress, resulting in localized regions of elevated stress within the material. To quantify the stress increase, the 99th percentile of the volume-weighted first principal stress in the matrix phase of each RVE was measured. This value was then used to compute a local stress increase factor by calculating the ratio between this percentile and the reference stress. In addition to the stress increase, an equivalent local stiffness is calculated for each RVE structure. By employing automated scripting, this procedure was iteratively applied to all RVEs, enabling the computation of a representative distribution of local stress increases across the material. Figure 4 shows the resulting distribution of stress increase from the simulation of approx. 400 RVEs of the B80 material.

The distribution of local stress increase is mapped to a distribution of fracture stresses which is used in damage simulations as discussed in the following section.

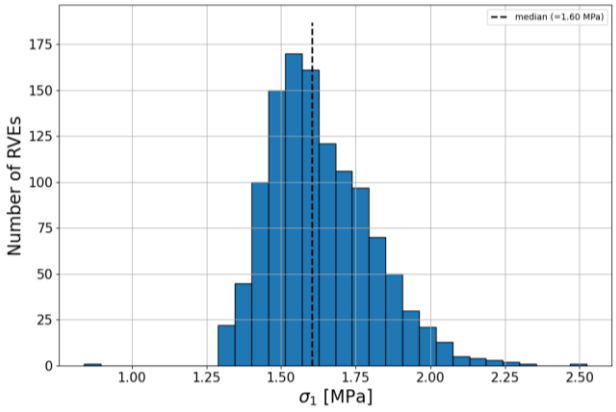

Fig. 4: Histogram of the stress increase of individual RVEs when applying an external tensile strain corresponding to a stress of 1 MPa to opposite faces of the RVE.

Macro-scale simulation of 3-point-bending

The scatter of bending strength of the refractory material is evaluated using a virtual three-point bending test as illustrated in Figure 5. The bending strength is computed using finite element analysis (FEA) with the goal of comparing it with experiments and eventually using FEA directly to evaluate the failure distribution of complex structures. The model accounts for microscopic elasticity via coupling the effective properties of the microscopic representative volume elements with a macroscopic model of a three-point bending test.

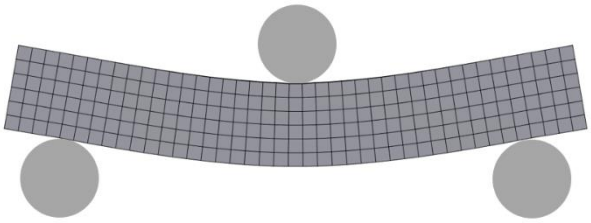

Fig. 5: Illustration of a finite element model of the three-point bending test.

On the macroscopic scale, an isotropic damage model that influences the stress-strain relationship is implemented as a user programmable feature (UPF) in Ansys [4, 5, 6]. The stress-strain relation is represented as

$$\boldsymbol{\sigma} = (1 - D)\,\mathbb{C}\,\boldsymbol{\varepsilon}\,,$$

where $\boldsymbol{\sigma}$ is the Cauchy stress tensor, $\boldsymbol{\varepsilon}$ denotes the strain tensor, $\mathbb{C}$ represents the fourth-order elasticity tensor and $D \in [0,1]$ is the damage variable, $D = 0$ corresponds to the undamaged state and $D = 1$ represents the fully damaged states.

The damage evolution is implicitly expressed by the following equation:

$$D(\kappa) = 1 - \frac{\kappa_0}{\kappa} e^{-\frac{\sigma_F h_e}{G_F}(\kappa - \kappa_0)},$$

where κ is the maximum value of the equivalent strain experienced during the loading history, κ_0 represents the critical equivalent strain beyond which damage is initiated, h_e represents the characteristic length associated with the element size in the FEA, σ_F represents the fracture stress, and G_F represents the fracture energy. A key point here is to use a modified equivalent von Mises strain from [5, 7] to evaluate κ. The modified version differentiates between tensile and compressive scenarios on the top and lower surfaces of the beam. This strain is given by the following expression:

$$\kappa = \frac{k-1}{2k(1-2\nu)} I_1 + \frac{1}{2k}\sqrt{\left(\frac{k-1}{1-2\nu} I_1\right)^2 + \frac{12k}{(1+\nu)^2} J_2}\,,$$

where ν represents the Poisson ratio, k represents the ratio of tensile to compressive strength, I_1 represents the first invariant of the strain tensor, and J_2 represents the second invariant of the deviatoric strain tensor. Moreover, the critical equivalent strain κ_0 is determined by

$$\kappa_0 = \sigma_F \frac{(1+\nu)(1-2\nu)}{E(1-\nu)}.$$

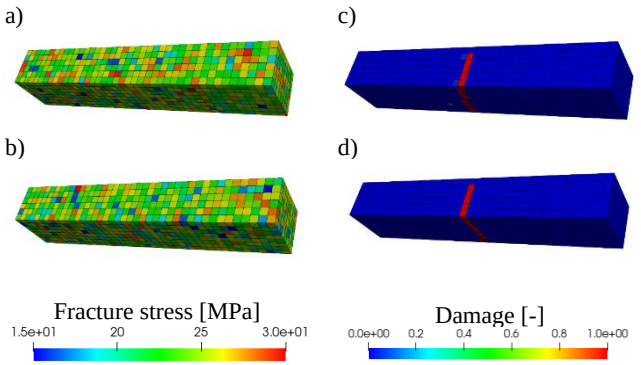

Fig. 6): a, b) fracture stress distribution of two randomly chosen beam models, where fracture stress in each element is coming from the underlying RVE. c, d) the corresponding damage evolution pattern given identical loading conditions.

To study the scatter of the bending strength and the effect of the microstructure on this scatter, various simulations are carried out with RVEs assigned in a random manner to each element of the beam model in order to reflect the inhomogeneous material/pore distribution. In other words, the material properties of each element come from a pool of RVEs resulting in beams with different fracture stress distributions, as seen in Figure 6a and Figure 6b.
Examining the corresponding damage distribution and crack path in Figure 6c and Figure 6d, the effect of the fracture stress distribution on the failure pattern and consequently on the bending strength (15.2 MPa and 14.9 MPa) can be seen. The fracture stress distribution around the center of the lower surface has a profound effect on the results as this is the location of the highest tensile stress. The simulation is run 45 times to allow statistical evaluation of the results. A Weibull distribution is fitted to the resulting bending stresses with a mean of 14.6 MPa and a standard deviation of 0.66 MPa. The mean is in good agreement with experimentally observed values of 14.8 MPa from in-house data. However, the standard deviation is further away from the experimental value of 1.25 MPa. The difference may be due to a limited fracture stress distribution that does not fully reflect reality. Further investigation could, for example, directly calculate the fracture stress in each RVE by simulation, thus reducing the dependence on the available experimental data.

CONCLUSIONS

We have presented a simulation-based approach to evaluating the failure probability of refractories for mechanical loads based on their microstructure composition. Using this method, it becomes possible to rapidly compare different refractory materials based on data from CT imagery, eliminating the need for costly and time-consuming destructive testing. This will enable more rapid iterations when designing new refractory materials. In a future work, more detailed investigation on the scatter of bending strength will be carried out and then the resulting failure distribution obtained using FEA will be validated against an experimental setup.

REFERENCES

[1] Isensee, F., Jaeger, P. F., Kohl, S. A., Petersen, J., & Maier-Hein, K. H. (2021). "nnU-Net: a self-configuring method for deep learning-based biomedical image segmentation." Nature methods, 18(2), 203-211.

[2] MPDB (Material Properties Database) v9.17, 2022. [Online], https://www.jahm.com/ (accessed 14 July 2023).

[3] P. Alliez, C. Jamin, L. Rineau, S. Tayeb, J. Tournois, and M. Yvinec, "3D Mesh Generation," in CGAL User and Reference Manual, 5.5.2 edition, CGAL Editorial Board, 2023. [Online], https://doc.cgal.org/5.5.2/Manual/packages.html#PkgMesh3 (accessed 14 July 2023).

[4] Ozaki, S., Nakamura, M., & Osada, T. (2020). Finite element analysis of the fracture statistics of self-healing ceramics. Science and Technology of Advanced Materials, 21(1), 609-625.

[5] Kurumatani, M., Terada, K., Kato, J., Kyoya, T., & Kashiyama, K. (2016). An isotropic damage model based on fracture mechanics for concrete. Engineering Fracture Mechanics, 155, 49-66.

[6] Oliver, J. (1989). A consistent characteristic length for smeared cracking models. International Journal for Numerical Methods in Engineering, 28(2), 461-474.

[7] Ozaki, S., Yamagata, K., Ito, C., Kohata, T., & Osada, T. (2022). Finite element analysis of fracture behavior in ceramics: Prediction of strength distribution using microstructural features. Journal of the American Ceramic Society, 105(3), 2182-2195.